Technological Trends: Aging in 20 Years

Drowsiness Monitoring with EEG-Based MEMS Biosensing Technologies

Chih-Wei Chang[1], Li-Wei Ko[1], Fu-Chang Lin[1], Tung-Ping Su[2], Tzyy-Ping Jung[1,3], Chin-Teng Lin[1], and Jin-Chern Chiou[1,4]

[1]National Chiao Tung University, Hsinchu, Taiwan, [2]Taipei Veterans General Hospital, Taipei, Taiwan, [3]University of California, San Diego, CA, USA, [4]China Medical University, Taichung, Taiwan

Abstract. Electroencephalography (EEG) has been widely adopted to monitor changes in cognitive states, particularly stages of sleep, as EEG recordings contain a wealth of information reflecting changes in alertness and sleepiness. In this study, silicon dry electrodes based on Micro-Electro-Mechanical Systems (MEMS) were developed to bring high-quality EEG acquisition to operational workplaces. They have superior conductivity performance, large signal intensity, and are smaller in size than conventional (wet) electrodes. An EEG-based drowsiness estimation system consisting of a dry-electrode array, power spectrum estimation, principal component analysis (PCA)-based EEG signal analysis, and multivariate linear regression was developed to estimate drivers' drowsiness levels in a virtual-reality-based dynamic driving simulator. The proposed system can help elders who are often affected by periods of tiredness and fatigue.

Keywords: aging, technology, cognitive state, drowsiness, dry electrode, EEG, MEMS, PCA

Electroencephalographic (EEG) signals consist of the differences in electrical potentials caused by summed postsynaptic graded potentials from pyramidal cells that create electrical dipoles between the soma (the body of a neuron) and apical dendrites (neural branches) (Teplan, 2002). Biopotential electrodes for EEG measurement transfer these biosignals from skin tissue to the amplifier circuit. Therefore, the most important characteristic of a biopotential electrode is low electrode-skin interface impedance so that signals can be propagated without attenuation or production of noise (Miller & Harrison, 1974).

When electrodes are placed on the skin of the forehead, an electrode-skin interface is constructed. The anatomy of the skin consists of three different layers: the epidermis, the dermis, and the subcutaneous layer. The epidermis contains two further layers: the stratum corneum (SC) and the stratum germinativum (SG). The SC consists of dead cells and thus has electrical isolation characteristics; the SG is composed of living cells and is therefore electrically conductive. Blood vessels and nerves are located in the dermis (Spence, 1990).

To overcome the electrical isolation properties of the SC, standard wet electrodes always require that the skin be prepared (abrasion of the SC) and an electrolytic gel be used. Improper skin preparation may cause skin irritation, pain, or even infection. Using electrolytic gel is uncomfortable and inconvenient; it can cause an itchy feeling, and sometimes makes the skin red and swollen when EEG measurements are made over a long period of time. Furthermore, the gel's conductivity gradually decreases because it hardens, resulting in degradation in the quality of data acquisition.

In this paper, the fabricated dry electrode is designed to pierce the SC in order to reach the electrically conducting tissue layer SG while not breaking through the dermis layer so as to avoid pain or bleeding. Since the dry electrode is expected to circumvent the high impedance characteristics of the SC, skin preparation and electrolytic gel application are thus not required. Note that the thickness of the epidermis varies from 0.05 mm to 1.5 mm depending on ethnicity and skin area, with the thickness of the SC and the SG reaching approximately 10–15 μm and 50–100 μm, respectively (Spence, 1990). Thus, in order to be able to pierce the SC and penetrate the SG, the probe must be longer than 20 μm and have a sharp tip to avoid any damage being caused during penetration. To reduce noise in the electrode-electrolyte interface, the probes are coated with titanium/platinum for high conductivity and biomedical capability. Three types of dry electrode arrays

DOI 10.1024/1662-9647/a000014

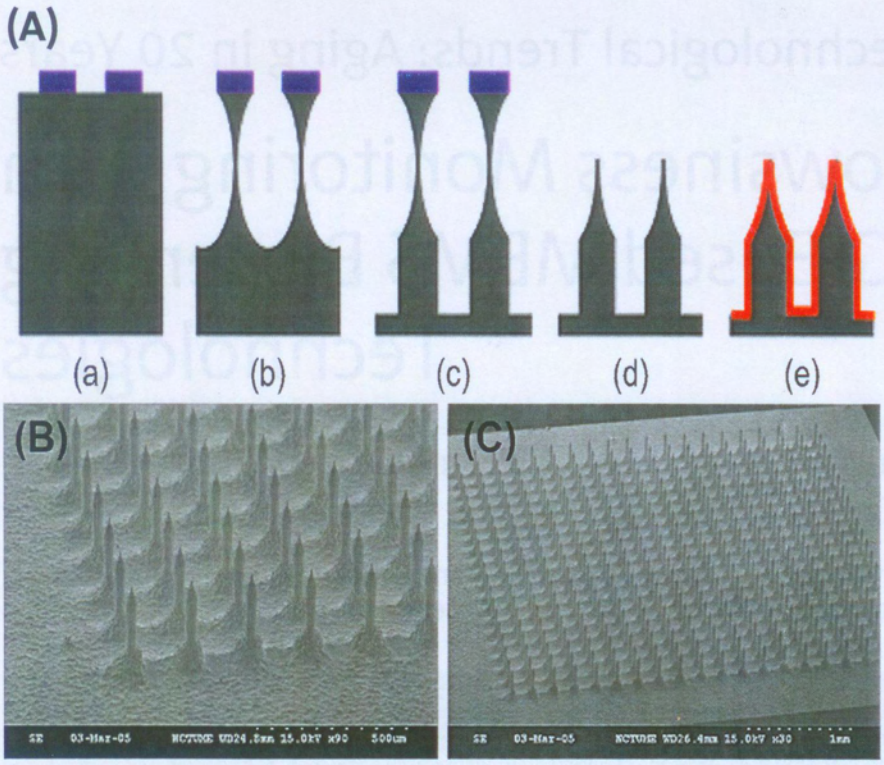

Figure 1. (A) Fabrication process: (a) photoresist pattern to provide etching masks; (b) isotropic etching carried out for probe tip; (c) anisotropic etching carried out for probe shaft; (d) hard mask released on the probe tip; (e) probes coated with titanium/platinum using DC-sputtering technique. (B) Structural electron microscopy of the fabricated dry electrodes. (C) A bird's eye view of whole electrode array.

consisting of 20 × 20 probes that are 4 mm × 4 mm, 3 mm × 3 mm, and 2 mm × 2 mm in size were fabricated for further comparisons. Due to the limitation of our current MEMS technology, these probes are approximately 250 µm in height and not capable of penetrating human hair in order to make contact with the stratum germinativum or even the stratum corneum. The elasticity of the hair also makes it difficult to fix the dry electrodes to the scalp. Therefore, in the current study, the dry electrodes are placed at hairless sites, such as frontal locations Fp1 and Fp2.

In order to evaluate the performance of the developed dry electrodes in realistic applications, we designed an attention-demanding experiment in which we continuously estimated subjects' drowsiness levels (task performance) based on the EEG signals measured by the dry electrodes.

This paper is structured as follows: First, we describe how the dry electrodes were fabricated. The following section describes how the dry electrodes were tested in characterization tests and in tests of the ability of the dry electrodes to acquire EEG data in a realistic driving task. We explored the application of dry electrodes in an EEG-based drowsiness estimation system as an example of a realistic application. The system comprises a virtual reality (VR)-based driving environment, a driving simulation cabin, a dynamic Stewart motion platform with six degrees of freedom (DOF), EEG power spectrum estimation, principal component analysis (PCA), and a linear regression model. Finally, we provide an outlook on this system's relevance for aging societies.

Fabrication of Dry Electrodes

To fabricate needle-like probes on a silicon wafer with high aspect ratio, a microfabrication process consisting of isotropic and anisotropic reactive ion etching with inductive coupled plasma (RIE-ICP) etching process and electroplating technology was developed and is illustrated in Figure 1A. In this process, a thick film of photoresist was patterned with circular dots to provide an etching hard mask for the cylindrical probes. Since the etching selectivity between silicon and photoresist is approximately 1 to 60, 6 µm thick photoresist was chosen as a protection hard mask for the two-stage isotropic/anisotropic etching processes. Upon completing the isotropic etching process for the probe tip, we proceeded with the anisotropic etching process so that a high aspect ratio probe shaft could be obtained. A wet-etching process was then used to release the hard mask at the probe tip. The probes were subsequently coated with titanium and platinum using a DC-sputtering technique in order to ensure electric conductivity. The dry electrodes were then cut out of the silicon wafer and mounted on flexible printed circuit board using silver glue. Figure 1B shows the scanning electron micrographs of the results of the dry electrode fabrication. Each dry electrode consists of a 20 × 20 micro-probe array; each probe is approximately 250 µm in height and 35 µm in diameter. A block bulge can be observed at the base of the probe at a height of about 50 µm, which is caused by the isotropic etching shape in the second fabrication process. Thus, the effective penetration length of the probe is about 200 µm. Figure 1C shows a bird's eye view of whole electrode array.

Table 1. Test patterns for measurement of electrode-skin-electrode impedance (ESEI)

Measurement series	1	2	3	4	5	6	7	8	9	10	11	12	13	14	15	16	17	18	19
Subject	1	1	1	2	2	2	3	3	3	4	4	4	4	4	5	5	5	5	5
Type	a	c	b	a	c	b	f	a	c	f	a	c	d	e	f	a	c	d	e

Notes. a = AgCl without skin preparation, b = AgCl with skin preparation, c = 4 mm × 4 mm without skin preparation, d = 3 mm × 3 mm without skin preparation, e = 2 mm × 2 mm without skin preparation, f = Au without skin preparation.

Testing of the Dry Electrodes

We divided the testing of the dry electrodes into two parts, first testing the dry electrodes in vivo, and then testing their applicability in a realistic setting.

Dry Electrode Characterization

To characterize the electrode-skin interface impedance effect, two electrodes were lined up on the forehead 4 cm apart from one another in order to perform the electrode-skin-electrode impedance interface (ESEI) experiments. A circuit proposed by Griss et al. (2001) was used to determine ESEI and to reduce the risk of harming the test person during biopotential recordings (Webster, 1998). A total of 19 tests were performed as shown in Table 1, involving five different test patterns to evaluate the performance of five different types of electrodes. These electrodes consisted of two standard wet electrodes coated with silver chloride (AgCl) and gold (Au) and 1 cm in diameter, and three fabricated dry electrodes of 4 mm × 4 mm, 3 mm × 3 mm, and 2 mm × 2 mm in size respectively.

First, we tested the impedance spectra between a 4 mm × 4 mm dry electrode with no skin preparation and electrolytic gel and an AgCl electrode with electrolytic gel, with or without skin preparation. Indeed, the impedance of the fabricated dry electrode for the EEG frequency range proved to be lower than the AgCl electrode, regardless of whether skin preparation had been conducted or not. Second, we evaluated all 5 electrodes (Au, AgCl, 4 mm × 4 mm, 3 mm × 3 mm, 2 mm × 2 mm) with no skin preparation and electrolytic gel. In the frequency range of interest for EEG (0.5–100 Hz), the average impedance of the MEMS dry sensors and the standard wet electrodes were 5.3 kΩ and 9.7 kΩ, respectively. Thus, the experiment showed that the impedance of the dry electrodes was superior to that of the wet electrodes.

Dry Electrodes Used for EEG Data Acquisition in a Realistic Driving Task

The growing number of traffic accidents has become a serious concern to society in recent years. Accidents caused by drivers becoming drowsy at the steering wheel have a high fatality rate because of the marked decline in drivers' perception, rec-

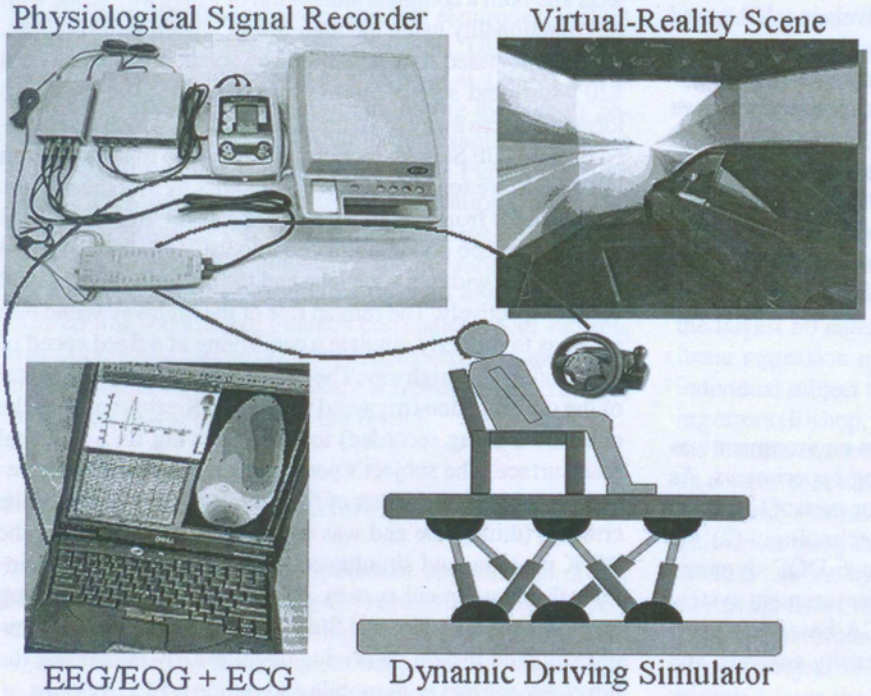

Figure 2. Block diagram of the dynamic VR-based driving simulation environment integrated with the EEG-based physiological measurement system.

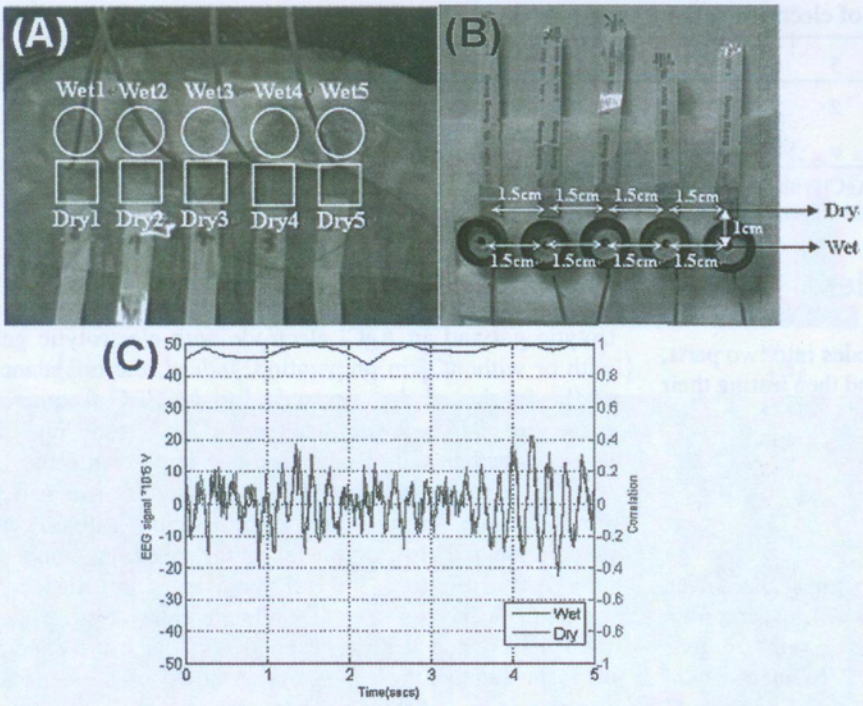

Figure 3. (A) Positions of wet and dry electrodes. (B) Relative distances between them. (C) Comparison of the EEG signals of presented dry and wet electrodes at Fp1 for Subject 1 during a 5-s segment. The upper line shows the Pearson correlation data calculated using 0.25-s segments.

ognition, and vehicle control abilities when they are sleepy. Preventing accidents caused by drowsiness is thus greatly desirable but requires techniques capable of continuously monitoring drivers' drowsiness levels and delivering effective feedback to avoid dangerous situations at the wheel (Amditis, Polychronopoulos, Bekiaris, & Antonello, 2002; Grace et al., 1998; Pilutti & Ulsoy, 1999; Ueno, Kaneda, & Tsukino, 1994; Wierwille, Wreggit, & Knipling, 1994). Recently, we proposed an EEG-based drowsiness estimation system that continuously estimates drivers' drowsiness levels in a VR-based driving simulator (Lin et al. 2006, 2007). Here, we used the same method to estimate subject drowsiness levels, but employed MEMS dry electrodes rather than conventional wet ones in order to acquire continuous EEG data. EEG power spectrum estimation, PCA-based EEG signal analysis and multivariate linear regression were applied to estimate drivers' drowsiness level in a VR-based dynamic driving simulator. The goal was to demonstrate the potential uses of the dry electrodes during long and routine recordings in operational environments.

VR-Based Driving Environ ment

A VR-based dynamic driving simulation environment was designed and built for interactive driving experiments. As shown in Figure 2, it includes four major parts: (1) the 3D highway driving scene based on VR technology, (2) the driving cabin simulator mounted on a 6-DOF dynamic Stewart motion platform, (3) the EEG measurement system with 13-channel sensors, and (4) the PCA-based EEG signal analysis approach, power spectral density analysis, and linear regression modeling.

The VR-based high-fidelity 3D interactive highway scene and its emulation software, WorldToolKit (WTK) library and application programmer's interface (API; Cardoso & Souloumiac, 2003), were presented previously (Lin et al., 2006, 2007). First, we created models of various objects (such as cars, roads, trees, etc.) for the scene and set up the corresponding positions, attitudes, and other relative parameters. We then developed the dynamic models among these virtual objects and built a complete simulation of a highway scene with full functionality using the high-level C-based API program.

The VR-based four-lane highway scene is projected on a 120 °-surround screen (304.1 cm wide and 228.1 cm high) located 350 cm away from the driving cabin, which is mounted on a 6-DOF Stewart motion platform. The four lanes from left to right are separated from one another by a median stripe. The distance from the left side to the right side of the road is divided into 256 points (digitized into values 0–255) of equal size, and the width of each lane and the car is 60 units and 32 units, respectively. The refresh rate of the highway scene was set so as to properly emulate a car driving at a fixed speed of 100 km/h on the highway. The car drifts away from the center of the cruising lane (triggered by the WTK program with the onset time being recorded) to mimic driving on a nonideal road surface. The subject's performance is defined as the deviation between the center of the vehicle and the center of the cruising (third) lane and was measured continuously by the WTK program and simultaneously recorded by the physiological measurement system. Based on the realistic driving environment, Lin, Ko, and Shen (2009) also proposed a new investigation insight on driving cognition, by integrating the novel dry sensors with mobile and wireless EEG systems.

Comparison of EEG Signals Acquired by Dry and Wet Electrodes

Figure 3A shows the placements of five dry/wet electrode pairs at the frontal locations. To test the EEG signal acquisition performance, we put the disposable dry and wet electrodes at hairless sites, such as Fp1 and Fp2 on the forehead area. The dry electrodes 1 and 5 were placed at Fp1 and Fp2 according to the international 10–20 electrode placement system (Thakor, 1998). We also placed three dry electrodes evenly between dry electrodes 1 and 5, and labeled them as Dry2, Dry3, and Dry4, respectively. As shown in Figure 3B, corresponding conventional wet electrodes were placed above the disposable dry electrodes and as close to them as possible (at about 1 cm distance). The common-reference recording derivations method was used to measure the EEG signals. In this method, three wet electrodes representing the reference and ground were used and placed at the A1, A2, and Gnd positions of the scalp. We used the average EEG signals at A1 and A2 as the reference. EEG signals at a total of 13 electrodes (5 dry electrodes, 5 wet ones, 2 reference and 1 ground channels) were then recorded simultaneously by the Scan NuAmps Express system (Compumedics Ltd., VIC, Australia). Before data acquisition, the contact impedance between each dry and wet electrode was calibrated to be less than 5 kΩ. The EEG data were recorded with a 16-bit quantization level at a sampling rate of 500 Hz and then resampled down to 250 Hz to simplify data processing. Each amplifier circuit channel had a differential-input instrumentation amplifier as the first amplifier stage, followed by a 0.5–100 Hz band pass filter and a 60 Hz notch filter.

We recruited three volunteers to take part in the experiment. In each experiment, the EEG signals were simultaneously recorded for 1000 s (about 16 min and 40 s) from the two pairs of disposable dry and wet electrodes, including eyes-open and eyes-closed conditions. Using the comparison method described by Matthews et al. (2007), a segment of a time-series recording comparing the signals obtained for Subject 1 from the pair of disposable dry and wet electrodes respectively at Fp1 is shown in Figure 3C. Also included on the plot is the Pearson correlation over 0.25-s segments. Although only a single 5-s segment is shown, the recording quality was consistent for all subjects without obvious changes in signal quality or noise levels. Statistics showed that the average Pearson correlation of all subjects was over 90%, and in 91% of the recording data it was higher than 92%. Very significant correlations, in excess of 90%, are evident throughout the record.

Drowsiness Estimation Performance

In order to demonstrate the potential applications of the MEMS electrodes during long and routine recording in operational environments, we investigated the quality of the EEG signals recorded by the dry electrodes placed at Fp1 and Fp2 to estimate subjects' drowsiness in an attention-demanding driving experiment. As shown in Figure 4, the EEG signals recorded by the 5 dry electrodes were fed into an EEG-based drowsiness estimation system to indirectly estimate the driver's drowsiness levels. The recorded driving performance time series were smoothed using a causal 90-s square moving-averaged filter (Steriade, 1993; Treisman, 1984) advancing at 2-s steps to eliminate variance at cycle lengths shorter than 1–2 min, since the fluctuations in drowsiness levels had a cycle length over 4 min (Jung, Makeig, Stensmo, & Sejnowski, 1997; Makeig & Jung, 1995). The EEG data recorded by 5 dry (or wet) electrode pairs were first preprocessed using a simple low-pass filter with a cutoff frequency of 50 Hz to remove the line noise and other high-frequency noise. After moving-average power spectral analysis, we obtained EEG log power spectrum time series from the 5 dry (or wet) electrode pairs, with a frequency range from 1 to 40 Hz (Grace et al., 1998). We then applied Karhunen-Loeve Principal Component Analysis (PCA) to the resultant EEG log spectrum to extract the directions of the largest variance for each session. Projections (PCA components) of the EEG log spectral data on the subspace formed by the eigenvectors corresponding to the largest 50 eigenvalues were used as inputs to a multiple linear regression model (Chatterjee & Hadi, 1986) for each individual subject to estimate the time course of his/her driving errors (Bishop, 1995). Each model was trained only using the features extracted from the training session and was tested on a separate testing session.

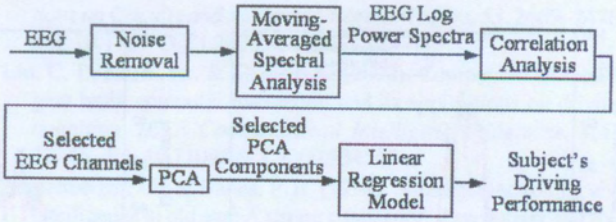

Figure 4. Flowchart representing the processing of the EEG signals: (1) A low-pass filter was used to remove the line noise and higher frequency (> 50 Hz) noise; (2) moving-averaged spectral analysis was used to calculate the EEG log power spectrum of each channel advancing at 2-s steps; (3) two EEG channels with higher correlation coefficients between the subject's driving performance and EEG log power spectrum were further selected; (4) PCA was trained and used to decompose selected features and extract the representative PCA components as the input vectors for the linear regression models; (5) the linear regression models were trained in one training session and used to continuously estimate and predict the individual subject's driving performance in the testing session.

Figure 5 shows the performance comparison of drowsiness estimation using dry electrodes. As illustrated in the figure, the dark line and light line represent the acquired and estimated driving errors respectively, with all of these figures representing test results. Figure 5A shows the estimated driving error of Subject 1 in Session 2 on the basis of the EEG signals recorded from the proposed dry electrodes. The estimators

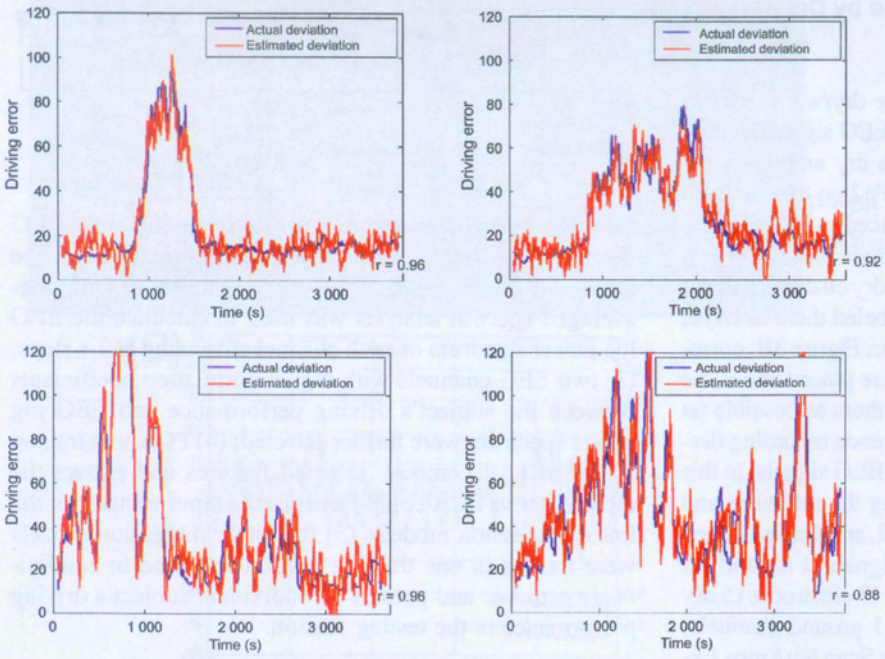

Figure 5. Estimated and actual driving errors based on the EEG signal recorded by the proposed dry electrode. (A) Subject 1 in Session 2 with estimators trained from Session 1 to estimate the driving error in Session 2. (B) Subject 1 in Session 1 with estimators trained from Session 2 to estimate the driving error in Session 1. (C) Subject 2 in Session 2 with estimators trained from Session 1 to estimate the driving error in Session 2. (D) Subject 2 in Session 1 with estimators trained from Session 2 to estimate the driving error in Session 1.

Table 2. Driving error correlation performance of the actual and EEG estimation in comparison with using dry and wet electrodes

	Session 1 estimates Session 2		Session 2 estimates Session 1	
	Wet electrode	Dry electrode	Wet electrode	Dry electrode
Subject 1	0.95	0.96	0.90	0.92
Subject 2	0.96	0.96	0.85	0.88

were trained using the EEG signals from Session 1 of Subject 1 to estimate the driving error in Session 2 (the red lines). Conversely, Figure 5B shows the estimated driving error of Subject 1 using EEG data from Session 2 as the training data set and those from Session 1 as the testing data set. Similarly, Figures 5C and Figure 5D show the estimated and actual errors made by Subject 2. Table 2 shows the comparison of the correlation coefficients between the actual and estimated driving error time series using dry and wet electrodes. As can be seen, the estimated driving errors (see Figure 5 and Table 2) compared well with the actual errors and were thus consistent with our previous report on the same driving tasks using whole-head 32-channel EEG (Lin et al., 2006, 2007). The results demonstrate the feasibility of accurately estimating subject drowsiness levels based on EEG signals collected from the frontal hairless sites. Furthermore, the estimation accuracy based on the EEG collected by dry electrodes is comparable to that based on the signals collected by conventional wet electrodes, indicating the feasibility of using dry electrodes to acquire EEG signals of a suitable quality without the need for skin preparation or conductive pastes in operational environments.

Outlook

Population aging is a worldwide phenomenon. The World Health Organization (WHO) has reported that there will be 1.2 billion people aged 60 and over by 2025. According to a projection made by the Council for Economic Planning in 2004, the number of people over 65 years will increase to 10% of the total population by 2011; furthermore, people over 75 years will amount to 43% of the population aged over 65. Although longevity is generally regarded as both a personal privilege and a medical achievement, extended average life expectancy and the resultant rapid increases in old and very old populations still represent a challenge to our society, particularly in terms of the cost of healthcare. This is compounded by the fact that gains in average physical longevity are not always accompanied by high levels of psychological, cognitive, and sensorimotor fitness, i.e., quality of life, in elders (Baltes & Baltes, 1990; Baltes & Lindenberger, 1997; Li et al., 2004; Lindenberger & Baltes, 1994). Societies need to seek ways to help old people maintain important psychological and physical functions so that their quality of life remains high, even in very old age (i.e., with possibilities of high degrees of mobility, independent living, and social networking). Cognitive-state monitoring based on biosensing technologies could be a way to identify cognitive deficits at an early stage and to take action by offering services and assistance.

Acknowledgments

The authors would like to thank Chia-Hsin Chung, Jong-Liang Jeng, and Chao-Yuen Hsu for their great help with

developing and implementing the experiments. This work was supported in part by the National Science Council, Taiwan, under contracts NSC 97-2627-E-009-001 and NSC 97-2221-E-009-138, in part by the Aiming for the Top University Plan of National Chiao Tung University, the Ministry of Education, Taiwan, under contract 98W962, and in part by the VGHUST Joint Research Program, Tsou's Foundation, Taiwan, under contract VGHUST98-G5–1.

References

Amditis, A., Polychronopoulos, A., Bekiaris, E., & Antonello, P. C. (2002). System architecture of a driver's monitoring and hypovigilance warning system. *IEEE Intelligent Vehicle Symposium, 2*, 527–532.

Baltes, P. B., & Baltes, M. M. (Eds.). (1990). *Successful aging: Perspectives from the behavioral sciences.* New York: Cambridge University Press.

Baltes, P. B., & Lindenberger, U. (1997). Emergence of a powerful connection between sensory and cognitive functions across the adult life span: A new window at the study of cognitive aging. *Psychology and Aging, 12,* 12–21. doi: 10.1037/0882-7974.12.1.12

Bishop, C. M. (1995). *Neural networks for pattern recognition.* Oxford: Oxford University Press.

Cardoso, J. F., & Souloumiac, A. (1993). Blind beamforming for non Gaussian signals. *Radar and Signal Processing, IEE Proceedings F, 140,* 362–370.

Chatterjee, S., & Hadi, A. S. (1986). Influential observations, high leverage points, and outliers in linear regression. *Statistical Science, 1,* 379–416. doi: 10.1214/ss/1177013622

Grace, R., Byrne, V. E., Bierman, D. M., Legrand, J. M., Gricourt, D., Davis, B. K. et al. (1998). A drowsy driver detection system for heavy vehicles. *Proceedings of the 1998 17th AIAA/IEEE/SAE Conference on Digital Avionics Systems, 2,* I36/1–I36/8. doi: 10.1109/DASC.1998.739878

Griss, P., Enoksson, P., Tolvanen-Laakso, H. K., Merilainen, P., Ollmar, S., & Stemme, G. (2001). Micromachined electrodes for biopotential measurements. *Journal of Microelectromechanical Systems, 10,* 10–16. doi: 10.1109/84.911086

Jung, T. P., Makeig, S., Stensmo, M., & Sejnowski, T. J. (1997). Estimating alertness from the EEG power spectrum. *IEEE Transactions on Biomedical Engineering, 44,* 60–69. doi: 10.1109/10.553713

Li, S.-C., Lindenberger, U., Hommel, B., Aschersleben, G., Prinz, W., & Baltes, P. B. (2004). Lifespan transformations in the couplings of mental abilities and underlying cognitive processes. *Psychological Science, 15,* 155–163. doi: 10.1111/j.0956-7976.2004.01503003.x

Lin, C. T., Chung, I. F., Ko, L. W., Chen, Y. C., Liang S. F., & Duann J. R. (2007). EEG-based assessment of driver cognitive responses in a dynamic virtual-reality driving environment. *IEEE Transactions on Biomedical Engineering, 54,* 1349–1352. doi: 10.1109/TBME.2007.891164

Lin, C. T., Ko, L. W., Chung, I. F., Huang, T. Y., Chen, Y. C., Jung, T. P. et al. (2006). Adaptive EEG-based alertness estimation system by using ICA-based fuzzy neural networks. *IEEE Transactions on Circuits and Systems: I. Regular Papers, 53,* 2469–2476. doi: 10.1109/TCSI.2006.884408

Lin, C. T., Ko, L. W., & Shen, T. K. (2009). Computational intelligent brain computer interaction and its applications on driving cognition. *IEEE Computational Intelligence Magazine, 4*(4), 32–46. doi: 10.1109/MCI.2009.934559

Lindenberger, U., & Baltes, P. B. (1994). Sensory functioning and intelligence in old age: A strong connection. *Psychology and Aging, 9,* 339–355. doi: 10.1037/0882–7974.9.3.339

Makeig, S., & Jung, T. P. (1995). Changes in alertness are a principal component of variance in the EEG spectrum. *NeuroReport, 7,* 213–216.

Matthews, R., McDonald, N. J., Anumula, H., Woodward, J., Turner, P. J., Steindorf, M. A. et al. (2007). Novel hybrid bioelectrodes for ambulatory zero-prep EEG measurements using multichannel wireless EEG system. *Lecture Notes in Artificial Intelligence, 4565,* 137–146. doi: 10.1007/978-3-540-73216-7

Miller, H. A., & Harrison, D. C. (1974). *Biomedical electrode technology.* New York: Academic Press.

Pilutti, T., & Ulsoy, G. (1999). Identification of driver state for lane-keeping tasks. *IEEE Transactions on Systems, Man and Cybernetics, Part A: Systems and Humans 29,* 486–502. doi: 10.1109/3468.784175

Spence, A. P. (1990). *Basic human anatomy.* Redwood City, CA: Benjamin Cummings.

Steriade, M. (1993). Central core modulation of spontaneous oscillations and sensory transmission in thalamocortical systems. *Current Opinion in Neurobiology, 3,* 619–625. doi: 10.1016/0959-4388(93)90064-6

Teplan, M. (2002). Fundamentals of EEG measurement. *Measurement Science Review, 2,* Section 2. Retrieved from http://www.measurement.sk/2002/S2/Teplan.pdf

Thakor, N. V. (1998) Biopotentials and electrophysiology. In J. G. Webster (Ed.), *The measurements, instrumentation, and sensors handbook* (Chap. 74). Boca Raton, FL: CRC Press.

Treisman, M. (1984). Temporal rhythms and cerebral rhythms. In J. Gibbon & L. Allen (Eds.), *Timing and time perception* (Vol. 423, pp. 542–565). New York: Academic Press.

Ueno, H., Kaneda, M., & Tsukino, M. (1994). Development of drowsiness detection system. *Vehicle Navigation and Information Systems Conference Proceedings*, 15–20. doi: 10.1109/VNIS.1994.396873

Webster, J. G. (1998). *Medical instrumentation application and design* (3rd ed.). New York: Wiley.

Wierwille, W. W., Wreggit, S. S., & Knipling, R. R. (1994). Development of improved algorithms for on-line detection of driver drowsiness. In *International Congress on Transportation Electronics: Leading change* (pp. 331–340). Warrendale, PA: Society of Automotive Engineers.

Jin-Chern Chiou

Brain Research Center and Department of Electrical Engineering
National Chiao Tung University
1001 University Road
Hsinchu, Taiwan 300
ROC
E-mail: chiou@mail.nctu.edu.tw